IIETA International Information and Engineering Technology Association
Advancing the World of Information and Engineering

TECNICA ITALIANA-Italian Journal of Engineering Science
Vol. 61+1, No. 2, December, 2018, pp. 143-150
Journal homepage: http://iieta.org/Journals/TI-IJES

Numerical study of MHD Prandtl-Eyring non-Newtonian fluid past a vertical plate in a non-Darcy porous medium

Funmilayo H. Oyelami[1*], Moses S. Dada[2]

[1] Department of Mathematical and Physical Sciences, Afe Babalola University, Ado Ekiti 360001, Nigeria
[2] Department of Mathematics, University of Ilorin, Ilorin 240101, Nigeria

Corresponding Author Email: adefolajufunmilayo@gmail.com

https://doi.org/10.18280/ti-ijes.620213

Received: 3 September 2018
Accepted: 16 October 2018

Keywords:
Prandtl-Eyring fluid, magnetic field, viscous dissipation, thermal radiation, magnetohydrodynamic, non-Newtonian

ABSTRACT

This work investigates along a vertical plate transient magnetohydrodynamic free convection flow of Prandtl-Eyring non-Newtonian fluid with non-Dacian properties in a medium that is permeable. Considering the effects of magnetic field, thermal radiation and viscous dissipation on the flow, the governing equations for the problem were formulated, non-dimensionalised and solved using the implicit finite difference scheme of Crank-Nicolson type. The finite difference equations formed Thomas algorithm tri-diagonal matrix system of equations, which were solved with the help of MATLAB programming package. Of great importance for this study are to investigate the influence of Prandtl-Eyring parameters and other physical parameters on the velocity, temperature and concentration profiles with the aid of graphs.

1. INTRODUCTION

In recent years, heat and mass transfer in boundary layer flow has gained attension as a result of its wide range of applications in nuclear engineering and industries. The results from this studies are used in modeling and simulation. Both thermal and concentration boundary layers develop when fluid at specified temperature and concentration flows over a surface that is at a different temperature and concentration.
Behaviour of non-Newtonian fluids in permeable medium varies due to different models used to analyse nonlinear relationship between shear stress and shear rate. For Prandtl-Eyring model, accordind to [1] the behaviour can be analysed using

$$\tau_{xy} = \omega sinh^{-1}\left(\frac{1}{b}\frac{\partial u}{\partial y}\right) \quad (1)$$

where ω and b corresponds to Prandtl-Eyring parameters, $\frac{\partial u^*}{\partial y^*}$ implies the rate of deformation, (x, y) are the Cartesian coordinates of any point in the flow domain and τ is the shear stress. Numerous practical applications and studies have brought about considerable interest in studying the flow of non-Newtonian fluids. [2-5] used Eyring-Powell model to analyze viscous behavior of non-Newtonian fluids. [6] investigated the non-Newtonian fluid flow under the effect of couple stresses between two parallel plates using Eyring-Powell model. Numerical study of viscous dissipation effect on free convection heat and mass transfer of magnetohydrodynamic (MHD) non-Newtonian fluid flow through a porous medium was carried out by [7]. [8] obtained boundary layer flow of an Eyring-Powell model fluid due to a stretching cylinder with a variable viscosity. Radiation effects on boundary layer flow of an Eyring-Powell fluid over an exponentially shrinking sheet was investigated by [9].

Few work has been done using Prandtl-Eyring non-Newtonian model. Review of non-Newtonian mathematical models for rheological characteristics of viscoelastic composites was carried out by [10]. Various constitutive equations are reviewed for a better understanding of their applicability to polymer melt in determining the viscosity.

Similarity analysis for natural convection boundary layer flow of Williamson and Prandtl-Eyring fluids using deductive group theoretic method was considered by [11]. They considered the velocity distribution, the slope of velocity and temperature variations for Prandtl-Eyring and Williamson fluid respectively. Their investigation showed that velocity and skin friction in Williamson fluids are considerably higher than those in Prandtl-Eyring. Unsteady magnetohydrodynamic flow showing comparison between Prandtl-Eyring and Eyring-Powell non-Newtonian fluid models on a parallel plate with wall slip effects through porous channel was studied by Oyelami and Dada [12]. Also, numerical investigations was carried out on non-Newtonian fluids along a vertical plate with emphasis on Eyring-Powell model by Oyelami and Dada [13].

In this present study, the effects of magnetic field, thermal radiation and viscous dissipation are considered on the transient free convection flow and of non-Newtonian fluids in porous media and the relationship between shear stress and rate of deformation was analysed using Prandtl-Eyring non-Newtonian fluid model.

2. FORMULATION OF PROBLEM

Transient free convection incompressible electrically conducting non-Newtonian Prandtl-Eyring fluid along a vertical plate in a saturated porous medium is considered. The x^*-axis is taken along the plate while the y^*-axis is taken normal to it. Along y^*-axis in the fluid flow, a magnetic field

of uniform strength was applied. Initially, at $t \leq 0$, it was assumed that both the plate and fluid are at the same temperature T_∞^* and concentration C_∞^*. At $t > 0$, the temperature and concentration of the plate was raised and both maintained T_w^* and C_w^* (greater than T_∞^* and C_∞^*). Along y^* direction, there is assumed to be a thermal radiation in form of unidirectional flux and other fluid properties were regarded as constant except for the approximation done by Boussinesq to body forces term in momentum equation. The Rosseland diffusion flux in the y^*according to [14] is defined as:

$$q_r = -\frac{4\sigma \partial T^{*4}}{3k^1 \partial y^*} \tag{2}$$

The governing equations for the above class of problem were formulated as follows:

$$\frac{\partial u^*}{\partial x^*} + \frac{\partial v^*}{\partial y^*} = 0; \tag{3}$$

$$\frac{\partial u^*}{\partial t^*} + u^* \frac{\partial u^*}{\partial x^*} + v^* \frac{\partial u^*}{\partial y^*} = \frac{1}{\rho}\frac{\partial}{\partial y^*}(\tau_{xy}) + g\beta_T(T^* - T_\infty^*) + g\beta_c(C^* - C_\infty^*) - \frac{\sigma B_0^2 u^*}{\rho} - \frac{\nu u^*}{k} - \frac{b u^{*2}}{k}; \tag{4}$$

$$\frac{\partial T^*}{\partial t^*} + u^* \frac{\partial T^*}{\partial x^*} + v^* \frac{\partial T^*}{\partial y^*} = \alpha \frac{\partial^2 T^*}{\partial y^{*2}} - \frac{1}{\rho C_p}\frac{\partial q_r}{\partial y^*} + \frac{\nu}{C_p}\left(\frac{\partial u^*}{\partial y^*}\right)^2 \tag{5}$$

$$\frac{\partial C^*}{\partial t^*} + u^* \frac{\partial C^*}{\partial x^*} + v^* \frac{\partial C^*}{\partial y^*} = D\frac{\partial^2 C^*}{\partial y^{*2}} - K_c(C^* - C_\infty^*) \tag{6}$$

with the following initial and boundary conditions:

$$\begin{aligned} &t^* \leq 0:\ u^* = 0, v^* = 0, T^* = T_\infty^*,\ C^* = C_\infty^*\ for\ every\ x^*\ and\ y^* \\ &t^* > 0: u^* = u_o^*,\ v^* = 0, T^* = T_w^*, C^* = C_w^* \quad at\ y^* = 0 \\ &u^* = 0,\ T^* = T_\infty^*,\ C^* = C_\infty^* \quad at\ x^* = 0 \\ &u^* \to 0, T^* \to T_\infty^*, C^* \to C_\infty^* \quad as\ y^* \to \infty. \end{aligned} \tag{7}$$

where T^*, C^*, u^* and v^* are temperature, concentration and velocities in x^* and y^* directions respectively, $\rho, g, t, \beta_T, \beta_C, \sigma, k, b, D, C_p, \alpha, B_o, K_c, q_r, \nu, \tau_{xy}$ are density, gravitational acceleration, time, thermal volumetric coefficient, concentration volumetric coefficient, electric conductivity, permeability, Darcy-Forchheimer, concentration diffusivity, specific heat, thermal diffusivity, magnetic field, chemical reaction, radiative heat flux, kinematic viscosity and stress tensor parameters respectively .

The series expansion for $\sin h^{-1}\left(\frac{1}{b}\frac{\partial u^*}{\partial y^*}\right)$ from the stress tensor for Prandtl-Eyring non-Newtonian fluid model modified after [4] defined in equation (1) gives

$$\sin h^{-1}\left(\frac{1}{b}\frac{\partial u^*}{\partial y^*}\right) \cong \frac{1}{b}\frac{\partial u}{\partial y} - \frac{1}{6}\left(\frac{1}{b}\frac{\partial u}{\partial y}\right)^3, \left|\frac{1}{b}\frac{\partial u}{\partial y}\right| \ll 1 \tag{8}$$

Hence, the stress tensor for Prandtl-Eyring model becomes

$$\tau_{xy} = \frac{\omega}{b}\frac{\partial u^*}{\partial y^*} - \frac{1}{6}\left(\frac{\omega}{b}\frac{\partial u^*}{\partial y^*}\right)^3 \tag{9}$$

With regards to Prandtl-Eyring non-Newtonian fluid model, the momentum equation is expressed as follows

$$\frac{\partial u^*}{\partial t^*} + u^*\frac{\partial u^*}{\partial x^*} + v^*\frac{\partial u^*}{\partial y^*} = \frac{\omega}{\rho b}\frac{\partial^2 u^*}{\partial y^{*2}} - \frac{\omega}{2\rho b^3}\left(\frac{\partial u^*}{\partial y^*}\right)^2\frac{\partial^2 u^*}{\partial y^{*2}} + g\beta_T(T^* - T_\infty^*) + g\beta_c(C^* - C_\infty^*) - \frac{\sigma B_0^2 u^*}{\rho} - \frac{\nu u^*}{k} - \frac{b u^*}{k} \tag{10}$$

This analysis concerns an optically thick limit boundary layers. For quartic function for sufficiently small temperature differences in the flow, the quartic temperature function following [15] can be expresses as a linear function of temperature by doing away with higher order terms as follows.

$$T^{*4} \approx 4T_\infty^{*3} - 3T_\infty^{*4} \tag{11}$$

Substituting the above equation into the Rosseland diffusion flux yields the following result for energy equation:

$$\frac{\partial T^*}{\partial t^*} + u\frac{\partial T^*}{\partial x} + v\frac{\partial T^*}{\partial y} = \alpha\frac{\partial^2 T^*}{\partial y^{*2}} + \frac{\nu}{\rho C_p}\left(\frac{\partial u}{\partial y}\right)^2 + \frac{16\sigma T_\infty^{*3}}{3k^1\rho c_p}\frac{\partial^2 T^*}{\partial y^{*2}} \tag{12}$$

To transform the dimensional governing equations, the following non-dimensional quantities are defined.

$$\begin{aligned} &x = \frac{x^* u_0^*}{\nu}, y = \frac{y^* u_0^*}{\nu}, u = \frac{u^*}{u_0^*}, t = \frac{t^* u_0^{*2}}{\nu}, T = \frac{T^* - T_\infty^*}{T_w^* - T_\infty^*}, C = \frac{C^* - C_\infty^*}{C_w^* - C_\infty^*}, Re = \frac{u_0^* l}{\nu}, Ec = \frac{u_0^{*2}}{C_p(T_w^* - T_\infty^*)}, Pr = \frac{\nu}{\alpha}, M = \frac{\sigma B_0^2 \nu}{\rho u_0^{*2}} \\ &Sc = \frac{\nu}{\alpha}, Da = \frac{k}{l^2}, R = \frac{k^1 k}{4\sigma T_\infty^{*3}}, Gr = \frac{g\beta_T(T_w^* - T_\infty^*)}{u_0^{*3}}, Gm = \frac{g\beta_c(C_w^* - C_\infty^*)}{u_0^{*3}} \end{aligned} \tag{13}$$

Introducing equation (13) into the dimensional equations (3), (4), (10) and (12) gives the following continuity, momentum, energy and concentration non-dimensional equations.

$$\frac{\partial U}{\partial X} + \frac{\partial V}{\partial Y} = 0 \tag{14}$$

$$\frac{\partial U}{\partial t} + U\frac{\partial U}{\partial X} + V\frac{\partial U}{\partial Y} = \left[\phi - \psi\left(\frac{\partial U}{\partial Y}\right)^2\right]\frac{\partial^2 U}{\partial Y^2} + G_r T + G_m C - MU - \frac{U}{D_a Re^2} - \frac{FsU^2}{DaRe} \tag{15}$$

$$\frac{\partial T}{\partial t} + U\frac{\partial T}{\partial X} + V\frac{\partial T}{\partial Y} = \frac{1}{Pr}\left(1 + \frac{4}{3N}\right)\frac{\partial^2 T}{\partial Y^2} + Ec\left(\frac{\partial U}{\partial Y}\right)^2 \tag{16}$$

$$\frac{\partial C}{\partial t} + U\frac{\partial C}{\partial X} + V\frac{\partial C}{\partial Y} = \frac{1}{Sc}\frac{\partial^2 C}{\partial Y^2} - \gamma C \tag{17}$$

with the following dimensionless boundary conditions

$$\begin{aligned} &t \leq 0:\ U = 0, \quad V = 0, \quad T = 0,\ C = 0\ for\ all\ X\ and\ Y \\ &t > 0:\ U = 1, V = 0, T = 1,\ C = 1 \quad at\ Y = 0 \\ &U = 0, T = 0, C = 0\ at\ X = 0 \\ &\mathrm{U} \to 0, T \to 0, \quad C \to 0\ as\ Y \to \infty \end{aligned} \tag{18}$$

where T is the dimensionless temperature, C is the dimensionless concentration, N is the thermal radiation parameter, Da is the Darcy number, Fs is the Forchheimer inertia number, Pr is the Prandtl number signifying the relative importance of heat conduction and viscosity of the fluid, Sc is the Schimdt number showing the ratio of momentum diffusivity and mass diffusivity, Re is the Reynold number, U

and V are dimensionless velocities in X and Y directions, t is the dimensionless time, Gr is the thermal Grashof number giving the relative importance of buoyancy forces to viscous forces, Gm is the concentration Grashof number, M is the Magnetic field parameter, Ec is the Eckert number characterizing the effect of dissipation, $\phi = \frac{\omega}{b\mu}$ and $\psi = \frac{\omega U_0^{*4}}{2\rho\nu^3 b^3}$ are the Prandtl-Eyring non-Newtonian parameters.

3. SOLUTION TO THE PROBLEM

Crank-Nicolson finite difference scheme was used to provide solution to the stated problem. The finite difference equation corresponding to the non- dimensional governing equations (14), (15), (16) and (17) are given as:

$$\frac{U_{i,j}^{k+1}-U_{i-1,j}^{k+1}+U_{i,j}^{k}-U_{i-1,j}^{k}+U_{i,j-1}^{k+1}-U_{i-1,j-1}^{k+1}+U_{i,j-1}^{k}-U_{i-1,j-1}^{k}}{4\Delta X}+\frac{V_{i,j}^{k+1}-V_{i,j-1}^{k+1}+V_{i,j}^{k}-V_{i,j-1}^{k}}{2\Delta Y}=0 \quad (19)$$

$$\frac{U_{i,j}^{k+1}-U_{i,j}^{k}}{\Delta t}+U_{i,j}^{k}\frac{\left(U_{i,j}^{k+1}-U_{i-1,j}^{k+1}+U_{i,j}^{k}-U_{i-1,j}^{k}\right)}{2\Delta X}+V_{i,j}^{k}\frac{\left(U_{i,j+1}^{k+1}-U_{i,j-1}^{k+1}+U_{i,j+1}^{k}-U_{i,j-1}^{k}\right)}{4\Delta Y}=\left[\phi-\psi\left(\frac{u_{j+1}^{k}-u_{j-1}^{k}}{2\Delta y}\right)^2\right]\frac{U_{i,j-1}^{k+1}-2U_{i,j}^{k+1}+U_{i,j+1}^{k+1}+U_{i,j-1}^{k}-U_{i,j}^{k}+U_{i,j+1}^{k}}{2(\Delta Y)^2}-\frac{1}{2DaRe^2}\left(U_{i,j}^{k+1}+U_{i,j}^{k}\right)-\frac{FsU_{i,j}^{k}}{2DaRe}\left(U_{i,j}^{k+1}+U_{i,j}^{k}\right)+\frac{Gr}{2}\left(T_{i,j}^{k+1}+T_{i,j}^{k}\right)+\frac{Gm}{2}\left(C_{i,j}^{k+1}+C_{i,j}^{k}\right)-\frac{M}{2}\left(U_{i,j}^{k+1}+U_{i,j}^{k}\right) \quad (20)$$

$$\frac{T_{i,j}^{k+1}-T_{i,j}^{k}}{\Delta t}+U_{i,j}^{k}\frac{\left(T_{i,j}^{k+1}-T_{i-1,j}^{k+1}+T_{i,j}^{k}-T_{i-1,j}^{k}\right)}{2\Delta X}+V_{i,j}^{k}\frac{\left(T_{i,j+1}^{k+1}-T_{i,j-1}^{k+1}+T_{i,j+1}^{k}-T_{i,j-1}^{k}\right)}{4\Delta Y}=\frac{1}{Pr}\left(1+\frac{4}{3N}\right)\frac{T_{i,j-1}^{k+1}-2T_{i,j}^{k+1}+T_{i,j+1}^{k+1}+T_{i,j-1}^{k}-T_{i,j}^{k}+T_{i,j+1}^{k}}{2(\Delta Y)^2}+Ec\left(\frac{U_{i,j+1}^{k}-U_{i,j-1}^{k}}{2\Delta Y}\right)^2 \quad (21)$$

$$\frac{C_{i,j}^{k+1}-C_{i,j}^{k}}{\Delta t}+U_{i,j}^{k}\frac{\left(C_{i,j}^{k+1}-C_{i-1,j}^{k+1}+C_{i,j}^{k}-C_{i-1,j}^{k}\right)}{2\Delta X}+V_{i,j}^{k}\frac{\left(C_{i,j+1}^{k+1}-C_{i,j-1}^{k+1}+C_{i,j+1}^{k}-C_{i,j-1}^{k}\right)}{4\Delta Y}=\frac{1}{Sc}\frac{C_{i,j-1}^{k+1}-2C_{i,j}^{k+1}+C_{i,j+1}^{k+1}+C_{i,j-1}^{k}-C_{i,j}^{k}+C_{i,j+1}^{k}}{2(\Delta Y)^2}-\frac{\gamma}{2}\left(C_{i,j}^{k+1}+C_{i,j}^{k}\right) \quad (22)$$

multiplying equations (19), (20), (21) and (22) by Δt for simplicity, the equations are arranged so that velocities, temperature and concentration at the present time step (k+1) are on the left while those of previous time step (k) are on the right hand side. Hence, the equation form tri-diagonal matrix system.

The grid point along the X direction is denoted by i while j and k are grid points along Y and t directions. Dividing X and Y into M and N grid gave a well-spaced points. Mesh sizes were taken to be ΔX=0.05, ΔY=0.25 and Δt=0.01 and the region of integration considered is a rectangle with sides Xmax=1.05 and Ymax=5.25 while Ymax lie outside the momentum, energy and concentration boundary layers.

While computing during a time step, the coefficients $U_{i,j}^{k}$and $V_{i,j}^{k}$ in the finite difference equation were taken to be constants. From the initial conditions at all grid points, the values of C, T, U and V are known. For the calculations of C, T, U and V at present time (k+1), the known values at previous time level (k) are used as follows:

Equation (22) on a given i- level at every internal nodal point forms a tri-diagonal system of equation. Thomas algorithm which was discussed in [3] was used to provide solution to the problem. With this, the value of C on a given i-level at time (k+1) level was known at every nodal point.

Also, the value of T at time (k+1) level was calculated in the same manner we calculated C using equation (21).

The results gotten from C and T at time (k+1) level are used in equation (20) to calculate U at time (k+1) level.

Hence, the values of C, T and U are known on a particular i level. This process was carried out several times at various i levels. This approach gave the values of C, T and U at all grid point.

The values of V were also calculated at every nodal point explicitly using equation (19) on a particular i level at (k+1) time level.

4. DISCUSSION OF RESULTS

In order to get more clue to the physical problem, fluid parameters were varied and their influence were studied on velocity, temperature and concentration distributions. Default values are given as: ϕ =2, ψ =0.5, Gr=15, Gm=15, M=1, γ=1, Da=0.1, Fs=0.1 Re=1, Pr=1.0, N=3.0, Ec=0.002, Sc=1.0 and all graph corresponds to these values except stated otherwise on the graph.

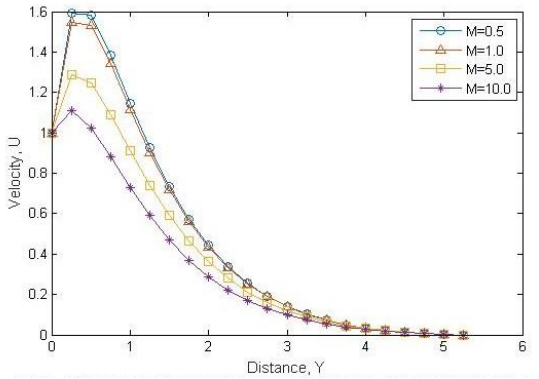

Figure 1. Velocity distribution for various values of thermal radiation parameter

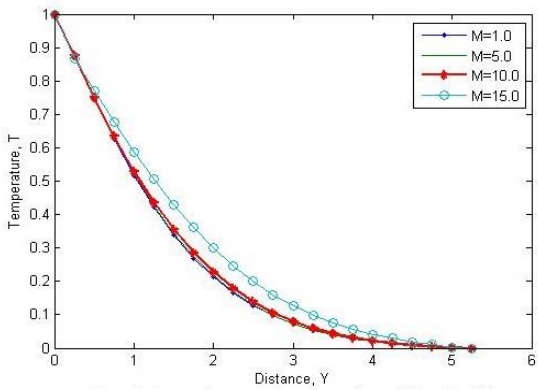

Figure 2. Temperature distribution for various values of thermal radiation parameter

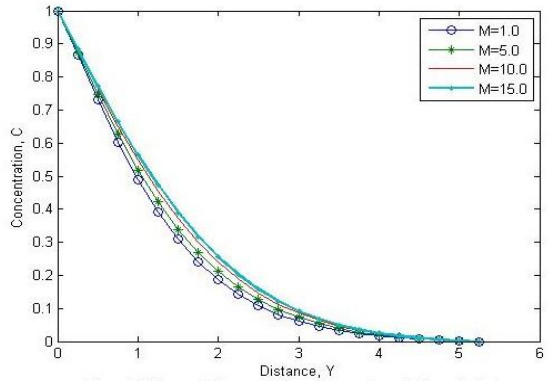

Figure 3. Concentration distribution for various values of thermal radiation parameter

Figures 1, 2 and 3 represent the effect of thermal radiation parameter N on the velocity, temperature and concentration distributions. A rise in N values results to a considerable reduction on velocity profile with reduction in velocity layers and transport of energy to the fluid. Temperature profile decreases while the concentration of the fluid increases with greater value of N and corresponding to smaller value of radiation flux.

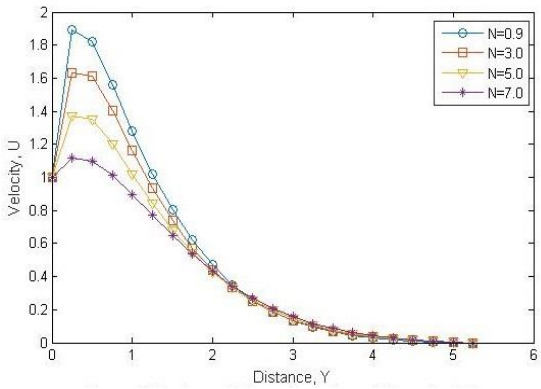

Figure 4. Velocity distribution for various values of Eckert number

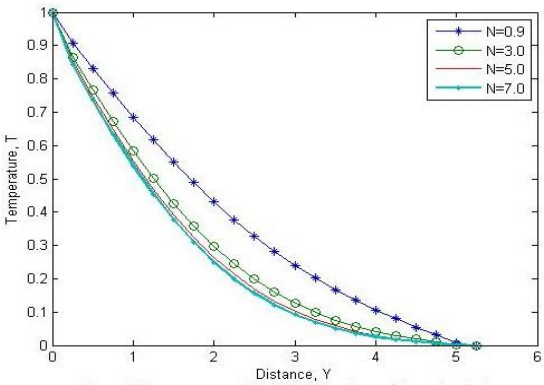

Figure 5. Temperature distribution for various values of Eckert number

The effect of increasing the viscous dissipation parameter Ec on velocity and temperature is presented on figures 4 and 5. With higher values of Ec, both the fluid velocity and temperature experienced a retarding effect with significant changes in both momentum and thermal boundary layer thicknesses.

Figures 6, 7 and 8 display magnetic field with various values on velocity, temperature and concentration distributions. Velocity distribution decreased on figure 6 as a result of increasing magnetic field parameters. This retarding effect is due to the presence of Lorentz force reducing the movement of the fluid. Temperature and concentration profiles rises with an increase in magnetic field parameters on figures 7 and 8 with little changes in the thermal and concentration boundary layers.

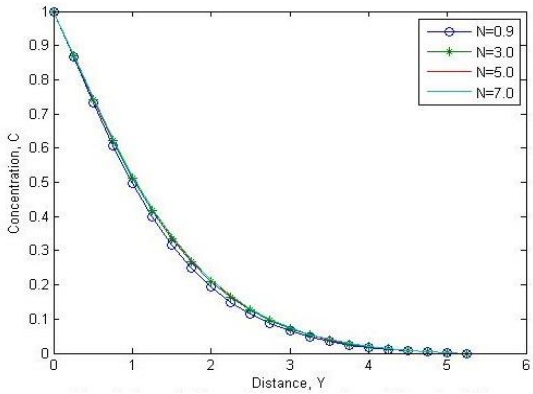

Figure 6. Velocity distribution for various values of magnetic field parameter

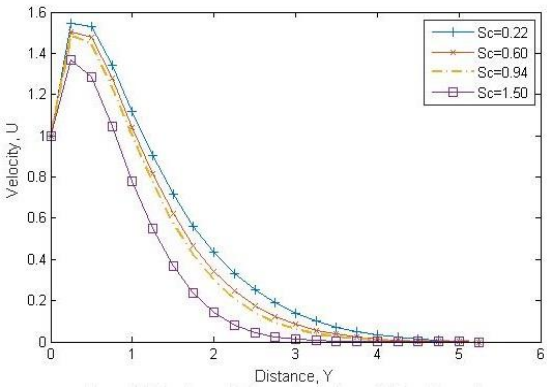

Figure 7. Temperature distribution for various values of magnetic field parameter

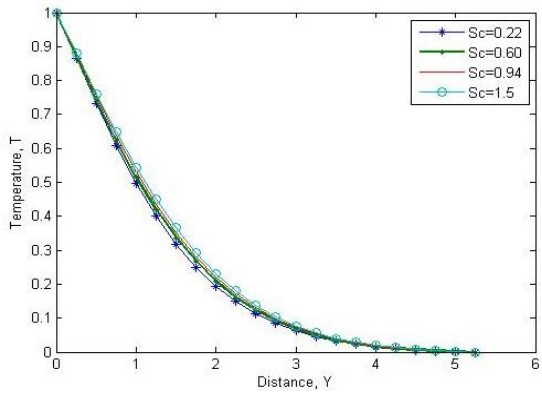

Figure 8. Concentration distribution for various values of magnetic field parameter

Figure 9, 10 and 11 represent the velocity, temperature and concentration profiles for Schmidt number Sc. A rise in Schmidt number decelerates the velocity and concentration

profiles. This decrease amounts to a reduced velocity, diffusivity and the concentration boundary layer thickness. This is because the ratio of thickness of the viscous and concentration boundary layer is measured by Schmidt number. Higher values of Sc gives lower diffusion properties. Concentration boundary layer becomes thinner than the velocity boundary layer thickness. Increase in Schmidt number causes a slight increase in the fluid temperature and the thermal boundary layer thickness.

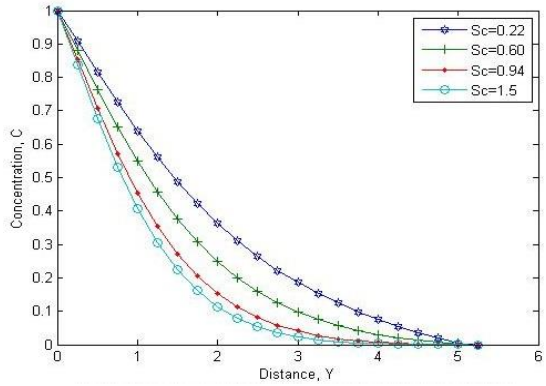

Figure 9. Velocity distribution for various values of Schmidt number

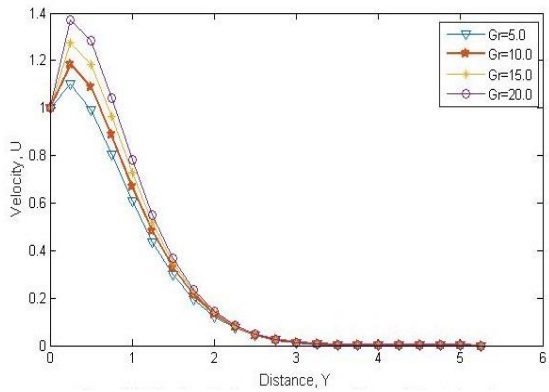

Figure 10. Temperature distribution for various values of Schmidt number

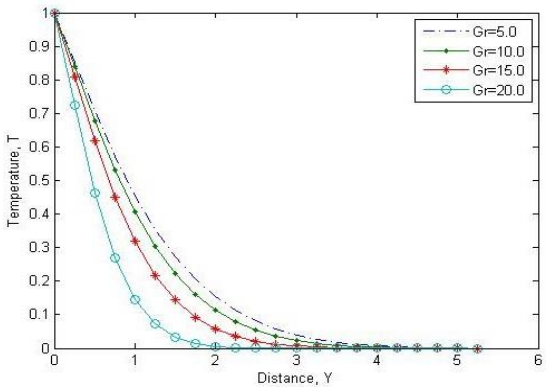

Figure 11. Concentration distribution for various values of Schmidt number

Figure 12, 13 and 14 depict the effect of thermal Grashof number Gr on velocity, temperature and concentration distributions. As Gr increases, velocity profile increases with a rise in buoyancy force and the velocity near the wall. On temperature profile, relative effect of increasing buoyancy force to viscous hydrodynamic force within the boundary layer decreases the temperature distribution. Concentration profile also decreases down the stream as shown on figure 14.

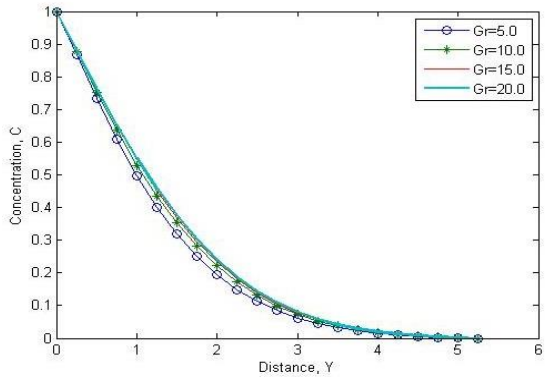

Figure 12. Velocity distribution for various values of thermal Grashof number

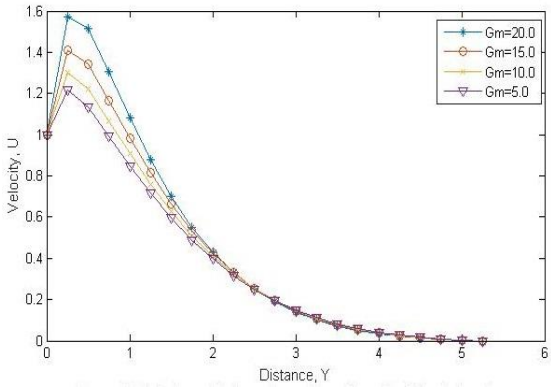

Figure 13. Temperature distribution for various values of thermal Grashof number

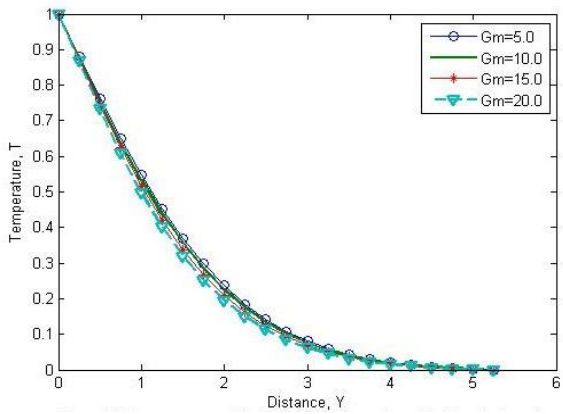

Figure 14. Concentration distribution for various values of thermal Grashof number

Figures 15 and 16 represent the importance of modified Grashof number Gm on the velocity and temperature distributions. Modified Grashof number Gm gives the relative importance of buoyancy force to the viscous forces and its effects on the velocity profile is seen to accelerate the magnitude of velocity of the flow. Increasing Gm leads to an increase in the velocity distribution while the fluid temperature decreases down the stream.

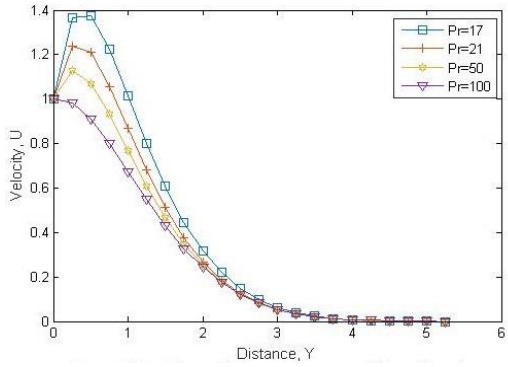

Figure 15. Velocity distribution for various values of modified Grashof number

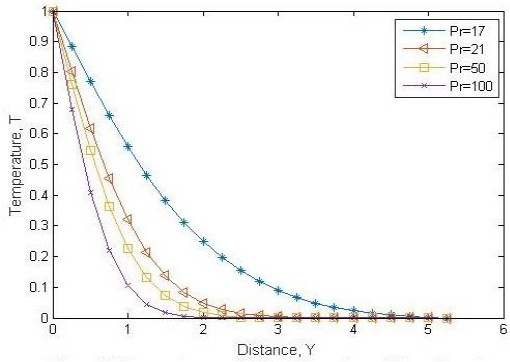

Figure 16. Temperature distribution for various values of modified Grashof number

Figures 17 and 18 show the effect of various Prandtl number Pr on velocity and temperature distributions. By signifying the thickness ratio of the viscous and thermal boundary layer thickness, a rise in the Pr values causes a decrease in the velocity and thermal boundary layer thickness. With smaller values of Pr, thermal conductivity of the fluid increases while higher value reaches zero faster.

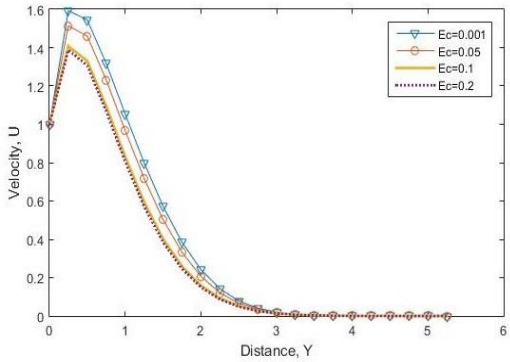

Figure 17. Velocity distribution for various values of Prandtl number

Figure 19 present the velocity distribution for various values of Prandtl-Eyring non-Newtonian parameter ϕ. It was discovered that parameter ϕ causes the flow rate of non-Newtonian fluid to below. Figure 20 shows the effect of the Prandtl-Eyring non-Newtonian parameter ψ on the velocity distribution. On this profile, an increase in non-Newtonian parameter ψ causes a rise in velocity distribution. However, from figures 19 and 20, we found that parameter ϕ accounts for the low rate of flow of Non-Newtonian fluids. Figures 21 and 22 represent the importance of permeability parameter Da on the velocity and temperature distributions. As Da increases, we experience an increase in the fluid temperature and a reduction in the velocity of the fluid because increasing the permeability increase the flow resistance reducing the fluid velocity and accelerating its temperature.

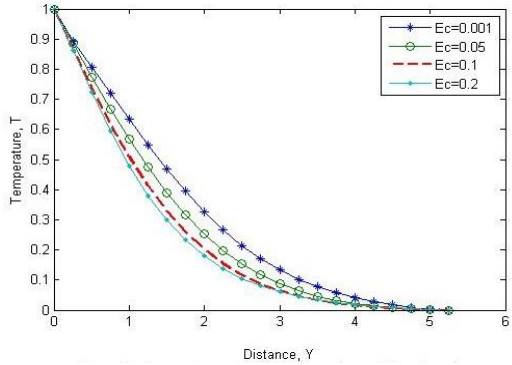

Figure 18. Temperature distribution for various values of Prandtl number

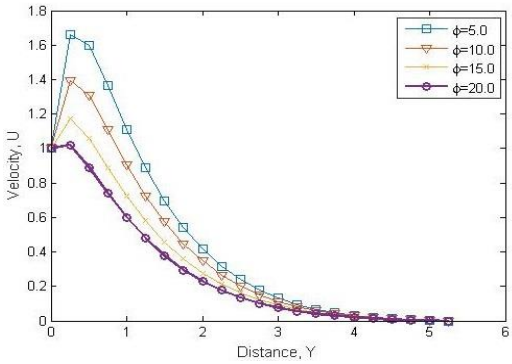

Figure 19. Velocity distribution for various values of Prandtl-Eyring parameter ϕ

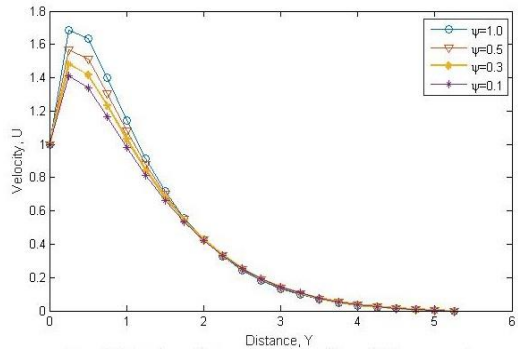

Figure 20. Velocity distribution for various values of Prandtl-Eyring parameter ψ

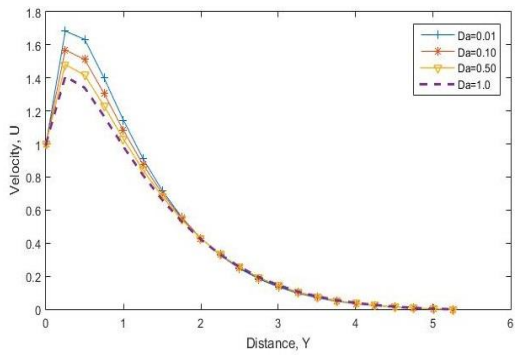

Figure 21. Velocity distribution for various values of Darcy number

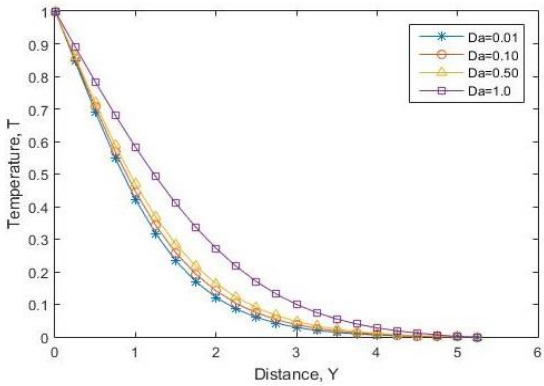

Figure 22. Temperature distribution for various values of Darcy number

5. CONCLUSION

In this study, transient incompressible magnetohydrodynamic Prandtl-Eyring non-Newtonian fluid in a porous medium, under the influence of thermal radiation, magnetic field and viscous dissipation was considered. The governing equations were simplified and non-dimensionalised. Solution was provided using implicit finite difference method of Crank Nicolson with the help of MATLAB programming package. The result show that:

A rise in thermal Grashof number, Non-Newtonian parameter ψ and modified Grashof number causes velocity distribution to increase while it reduces as dissipation function, non-Newtonian parameter ϕ, magnetic field parameter, Darcy number, thermal radiation parameter, Schmidt number and Prandtl number increases.

Temperature rises as magnetic field and Schmidt number increases while it reduces as Prandtl number, thermal Grashof number, modified Grashof number, thermal radiation and viscous dissipation parameter increases.

Increase in Schmidt number, thermal Grashof number and magnetic field causes a decrease in Concentration profile.

REFERENCES

[1] Wilkinsion WL. (1960). Non-Newtonian fluids. Pergamon Press, N. Y.

[2] Islam S, Shah A, Zhou CY, Ali I. (2009). Homotopy pertubation analysis of slider bearing with Powell-Eyring fluid. Z. Angew. Math. Phys. 60: 178-1193. https://doi.org/10.1007/s00033-009-7034-9

[3] Patel M, Timol MG. (2009). Numerical treatment of Powell Eyring fluid flow using method of asymptotic boundary conditions. Appl. Numer. Math. 59: 2584-2592. https://doi.org/10.1016/j.apnum.2009.04.010

[4] Patel M, Timol MG. (2011). Numerical treatment of MHD Powell Eyring fluid flow using method of satisfaction of asymptotic boundary conditions. Int. J. Math. Sci. Comput. 2: 71-78.

[5] Hayat T, Iqbal Z, Qasim M, Obaidat S. (2012). Steady flow of an Eyring Powell fluid over a moving surface with convective boundary conditions. Int. J. Heat Mass Transfer 55: 1817-1822. https://doi.org/10.1016/j.ijheatmasstransfer.2011.10.046

[6] Eldaebe NTM, Hassan AA, Mona AA. (2003). Effect of couple stresses on the MHD of a non-Newtonian unsteady flow between two parallel porous plates. Journal of physics 58a: 204-210.

[7] Eldabe NTM, Sallam SN, Abou-zeid MY. (2012). Numerical study of viscous dissipation effect on free convection heat and mass transfer of MHD non-Newtonian fluid flow through a porous medium. Journal of the Egyptian Mathematical Society 20: 139-151. https://doi.org/10.1016/j.joems.2012.08.013

[8] Malik AY, Hussian A, Nadeem S. (2013). Boundary layer flow of an Eyring-Powell model fluid due to a stretching cylinder with a variable viscosity. Journal of Scientia Iranica 20(2): 313-321.

[9] Ara A, Khan Najeeb A, Khan H, Sultan F. (2014). Radiation effects on boundary layer flow of an Eyring-Powell fluid over an exponentially shrinking sheet. Ain Shams Engineering Journal 5: 1337-1342. https://doi.org/10.1016/j.asej.2014.06.002

[10] Cherizoll R, Sain1 M, Tjong J. (2015). Review of non-newtonian mathematical models for rheological characteristics of viscoelastic composites. Green and Sustainable Chemistry 5: 6-14.

[11] Darji RM, Timol MG. (2013). Group-theoretic similarity analysis for natural convection boundary layer flow of a class of non-newtonian fluids. International Journal of Advanced Scientific and Technical Research 3(1): 54-69.

[12] Oyelami FH, Dada MS. (2018). Unsteady magnetohydrodynamic flow of some non-Newtonian fluids with slip in a porous channel. International Journal of Heat and Technology 36(2): 709-713. https://doi.org/10.18280/ijht.360237

[13] Oyelami FH, Dada MS. (2018). Numerical analysis of non-Newtonian fluid in a non-Darcy porous channel. International Journal of Heat and Technology 87(2): 83-91. https://doi.org/10.18280/mmc_b.870204

[14] Modest M.F. (1993). Radiation heat transfer. MacGraw-Hill, New York.

[15] Rapits A, Perdikis C. (2004). Unsteady flow through a highly porous medium in the presence of radiation. Transport Porous Media 57(2): 171- 179.

NOMENCLATURE

X, Y	Non-dimensional coordinate along and normal to the plate
U, V	Non-dimensional velocities in X and Y directions
N	Thermal radiation parameter
P^*	Dimensional pressure
P	Dimensionless fluid pressure
T^*	Dimensional temperature of fluid
T	Dimensionless temperature of fluid
C^*	Dimensional concentration of fluid
C	Non-dimensional concentration of fluid
ϕ, ψ	Prandtl-Eyring parameters
B_0	Applied magnetic field
C_p	specific heat at constant pressure
D_a	Darcy number
E_c	Eckert number
G_r	Thermal Grashof number
P_r	Prandtl number
q_r	radiative heat flux
R_e	Reynolds number

t^*	Dimensional time
t	Non-dimensional time
x^*, y^*	Dimensional coordinates along and normal to the plate
u^*, v^*	Dimensional velocities in $x^*$and y^* directions
g	gravitational acceleration
k	permeability
u	Velocity in the x direction
v	Velocity in the y direction
N	Thermal radiation parameter
P^*	Dimensional pressure
P	Non-dimensional fluid pressure
T_w	Temperature of the plate
C_w	Concentration of the plate

Greek alphabets

ρ	density
σ	Stefan-Boltzmann constant
a, c	characteristic of Eyring-Powell model
μ	Viscosity
τ_{xy}	stress tensor
β_T and β_C	thermal volumetric coefficient and concentration volumetric coefficient